nature geoscience

ARTICLES

PUBLISHED ONLINE: 30 JANUARY 2017 | DOI: 10.1038/NGEO2887

Elevated atmospheric escape of atomic hydrogen from Mars induced by high-altitude water

M. S. Chaffin*, J. Deighan, N. M. Schneider and A. I. F. Stewart

Atmospheric loss has controlled the history of Martian habitability, removing most of the planet's initial water through atomic hydrogen and oxygen escape from the upper atmosphere to space. In standard models, H and O escape in a stoichiometric 2:1 ratio because H reaches the upper atmosphere via long-lived molecular hydrogen, whose abundance is regulated by a photochemical feedback sensitive to atmospheric oxygen content. The relatively constant escape rates these models predict are inconsistent with known H escape variations of more than an order of magnitude on seasonal timescales, variation that requires escaping H to have a source other than H_2. The best candidate source is high-altitude water, detected by the Mars Express spacecraft in seasonally variable concentrations. Here we use a one-dimensional time-dependent photochemical model to show that the introduction of high-altitude water can produce a large increase in the H escape rate on a timescale of weeks, quantitatively linking these observations. This H escape pathway produces prompt H loss that is not immediately balanced by O escape, influencing the oxidation state of the atmosphere for millions of years. Martian atmospheric water loss may be dominated by escape via this pathway, which may therefore potentially control the planet's atmospheric chemistry. Our findings highlight the influence that seasonal atmospheric variability can have on planetary evolution.

Hydrogen loss has substantially impacted the water inventory of Mars, with D/H ratios in near-surface water indicating that perhaps five-sixths of the planet's initial water has escaped to space[1–5]. This escape is sourced in part from near-surface odd-hydrogen chemistry in which water photolysis products catalyse the recombination of CO_2 (refs 6–11). A by-product of this catalysis is molecular hydrogen, whose chemical lifetime is measured in centuries, and which accounts for approximately 10–20 ppm of the atmosphere at the surface[12]. Unlike water, which is typically assumed in models to be cold trapped by low temperatures at the tropopause, H_2 can migrate into the upper atmosphere, where some fraction is dissociated, diffuses to the exobase as H, and escapes. Standard models predict that because H escape is predominantly sourced from long-lived molecular hydrogen, variations as a function of season or solar cycle are typically less than a factor of two[13,14]. In addition, because the H_2 production rate decreases with increasing atmospheric abundance of O_2, a feedback operating on million-year timescales tends to set the hydrogen escape rate to twice that of oxygen[6,15], a fact many authors have used to conclude that the total time-integrated loss of H is twice that of O (refs 16,17). One conclusion of the present work is that this inference is flawed.

Observations of enhanced and variable H escape by Mars Express[18] and the Hubble Space Telescope[19,20] reveal that H escape cannot be sourced from molecular hydrogen alone, requiring direct water transport to the upper atmosphere. The Mars Express observations indicate that the flux of H declined by at least a factor of 10 over six months in late Mars Year 28 (July–December 2007), during the decay of a global dust storm in southern autumn as Mars moved away from perihelion. Over this timespan, general circulation model calculations predict at most a factor of five decline due to lower extreme ultraviolet heating at greater Mars–Sun distances[21]. The highest escape fluxes derived from the Mars Express observations ($>10^9$ cm^{-2} s^{-1}) exceed by a factor of two the maximum flux at which lower atmospheric diffusion of H_2 can supply H to the upper atmosphere ($\sim 2 \times 10^8$ cm^{-2} s^{-1})[9], assuming the H_2 abundance of the lower atmosphere is that reported by ref. 12. Another source molecule is therefore required to carry H to the upper atmosphere and supplement H escape. Water is the best candidate, both because it is the major atmospheric H reservoir and because such water has been detected between 40–100 km using SPICAM solar occultations[22,23]. Furthermore, water has been inferred to have a non-zero flux into the thermosphere using MAVEN measurements of H-bearing ionospheric species[24]. Taken together, these studies indicate that water is not as efficiently cold trapped as models typically assume. Efforts have been made to determine the production mechanism, spatial extent and longevity of this water[25–27], but its impact on escape has never previously been quantified.

Photochemical model response to high-altitude water

To determine whether observed upper atmospheric water could account for the observed variations in H escape, we built a new one-dimensional time-dependent photochemical model. We use this model to determine the time response of the atmosphere to different prescribed water profiles. See Methods for additional details, and Supplementary Tables 1 and 2 for the reaction network and boundary conditions used. Our standard water vapour profile is well mixed in the lower troposphere, tracks the saturation vapour pressure to a minimum concentration near the tropopause, and is fixed to this minimum mixing ratio at higher altitudes, containing a total of 6.94 precipitable micrometres of water vapour. With this profile the model reproduces the equilibrium photochemistry of the atmosphere as reported in prior studies (Fig. 1a), establishing model stability. In equilibrium, H and O escape rates are stoichiometrically balanced at 2:1.

To assess the atmospheric response to high-altitude water, we depart from the equilibrium steady state by adding water vapour to the standard profile in a Gaussian parcel with an altitude of 60 km and a concentration of 80 ppm. The resulting profile is

Laboratory for Atmospheric and Space Physics, University of Colorado, Boulder, Colorado 80303, USA. *e-mail: michael.chaffin@colorado.edu

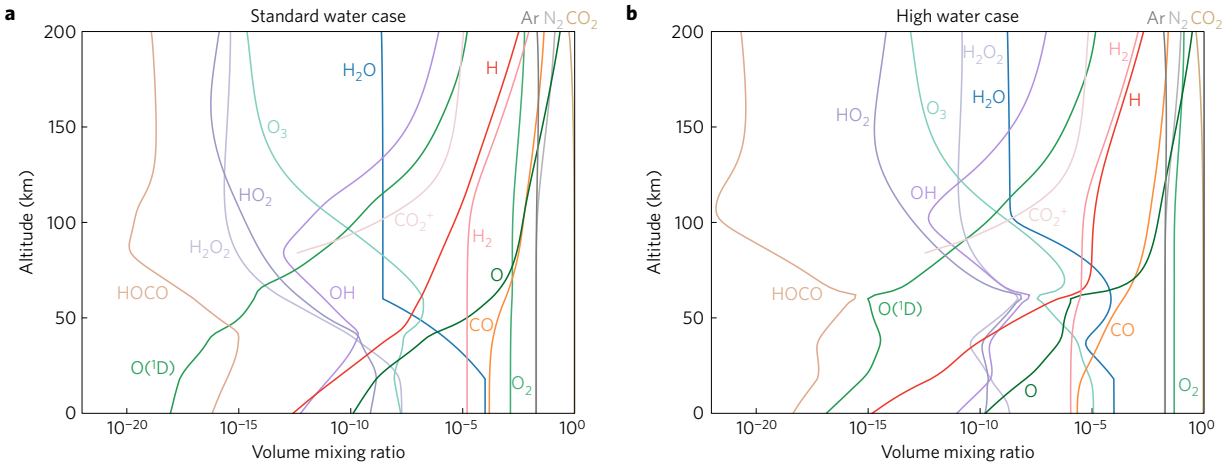

Figure 1 | Equilibrium photochemical model output. All model species are shown as a fraction of the total atmosphere at all model altitudes (see Supplementary Fig. 2 for absolute densities). **a**, The model reproduces the well-known photochemistry of the Mars atmosphere for a standard water profile. Long-lived species such as H_2 have constant mixing ratios in the well-mixed lower atmosphere and follow their own scale height above the homopause. **b**, With the introduction of upper atmospheric water, the equilibrium photochemistry is greatly perturbed. Compared with the standard model, the abundance of molecular oxygen is greatly increased, the O_2/CO ratio is much larger, and the abundance of hydrogen resulting from water breakdown is decreased in the lower atmosphere.

similar to concentrations observed by ref. 23 on Mars Express Orbit 6857, which covered southern mid-latitudes in summer ($L_s \approx 250$, Supplementary Fig. 1). The total water added is 0.03 precipitable micrometres, less than 1% of the original column. Running the system to equilibrium, a process that takes ~10 Myr of simulated time, we obtain an endmember case for the impact of high-altitude water on atmospheric chemistry (Fig. 1b). The water-enhanced atmosphere shows several notable differences from the standard case, including a much higher abundance of O_2, a higher O_2 to CO ratio, a decreased molecular hydrogen abundance, and a higher concentration of atmospheric ozone. Once equilibrium is reached, the escape of H and O is again stoichiometrically balanced—but a large imbalance is present before the system equilibrates, as we discuss below.

Time response of the atmosphere to water introduction

We determine the timescale of the atmospheric response to water injection by instantaneously introducing a water vapour enhancement into our standard equilibrium case and running it for one Earth year (roughly half of a Mars year) to determine the seasonal response of the atmosphere. After this we return to the nominal profile and track the relaxation of the atmosphere for an additional Earth year (Fig. 2). Instantaneous introduction and continuous maintenance of the parcel are assumed but not likely; we defer a more realistic accounting for the transport and dissociation of this water to a future study and consider our simulations a benchmark for the atmospheric response.

Following introduction of the parcel, the atomic and subsequently molecular hydrogen concentration increases as a result of local photodissociation at high altitude. Meanwhile, enhanced CO_2 recombination occurs at the altitude of the water bulge, decreasing the O and CO concentrations. After ten days (roughly the transport timescale at the parcel altitude), the H density increase at 200 km produces a factor of 10 increase in H escape. Over the next year, further increases in H escape are small compared with the prompt response. Removing the water enhancement at altitude restores the initial atmospheric conditions within a year, with a prompt factor of 10 decrease in H escape in the first ten days. Over the same time period O is reintroduced at middle altitudes thanks to less efficient CO_2 recombination in the absence of water.

The large escape of H in this time period is not in stoichiometric balance with O. After returning to the normal water profile, a small amount of residual oxygen is left in the atmosphere. This O does not strongly affect O escape rates, because O escapes predominantly by dissociative recombination of O_2^+, which is already the major ion in the ionosphere, and whose concentration is controlled more by solar extreme ultraviolet irradiation than atmospheric composition[28]. Instead, excess atmospheric O slightly increases O_2 concentrations, incrementally suppressing H_2 production. If left in this state, the atmosphere would lose H at an infinitesimally lower rate over the next several million years, until the integrated loss of H and O reached stoichiometric balance and the original slightly higher H escape rate was restored. If instead the water perturbation recurred every southern summer, representing a net addition to the starting water profile, the atmosphere would consistently lose more H than O until an equilibrium atmosphere intermediate to those in Fig. 1 was attained, in which H and O escape is balanced over the Martian year. This restoration of equilibrium after millions of years does not recover the H lost before balance is restored (see Supplementary Fig. 3): the net effect of departing from a steady state and adding high-altitude water to the system is the escape of more H than O. Loss of H relative to O is therefore a natural consequence of the departure from an atmospheric steady state, as has been occasionally recognized in the past (see ref. 29); we discuss this further in the conclusions and Supplementary Methods.

To understand the effects of upper atmospheric water more generally, we simulated the response to a range of introduced water profiles over the first 10^7 s of simulated time (Fig. 3). Numerical details of the atmospheric response are given in Supplementary Table 3. For completeness, we ran each of these profiles for 10^9 yr, until each atmosphere reattained photochemical equilibrium (see Supplementary Fig. 3).

Because we add water as a fraction of the bulk atmosphere (replicating the likely consequence of transport), increasing the altitude of the perturbation reveals competing effects. At first, higher altitudes accelerate photodissociation of the water vapour into odd hydrogen, enhancing escape. For water introduced above 80 km, the H escape response decreases because the absolute amount of water introduced by the perturbation in mixing ratio is smaller. Independent of the magnitude of the escape enhancement, water introduced at higher altitudes results in shorter response times.

In our studies, H escape is insensitive to large changes in lower atmospheric water vapour below 20 km on year-long timescales,

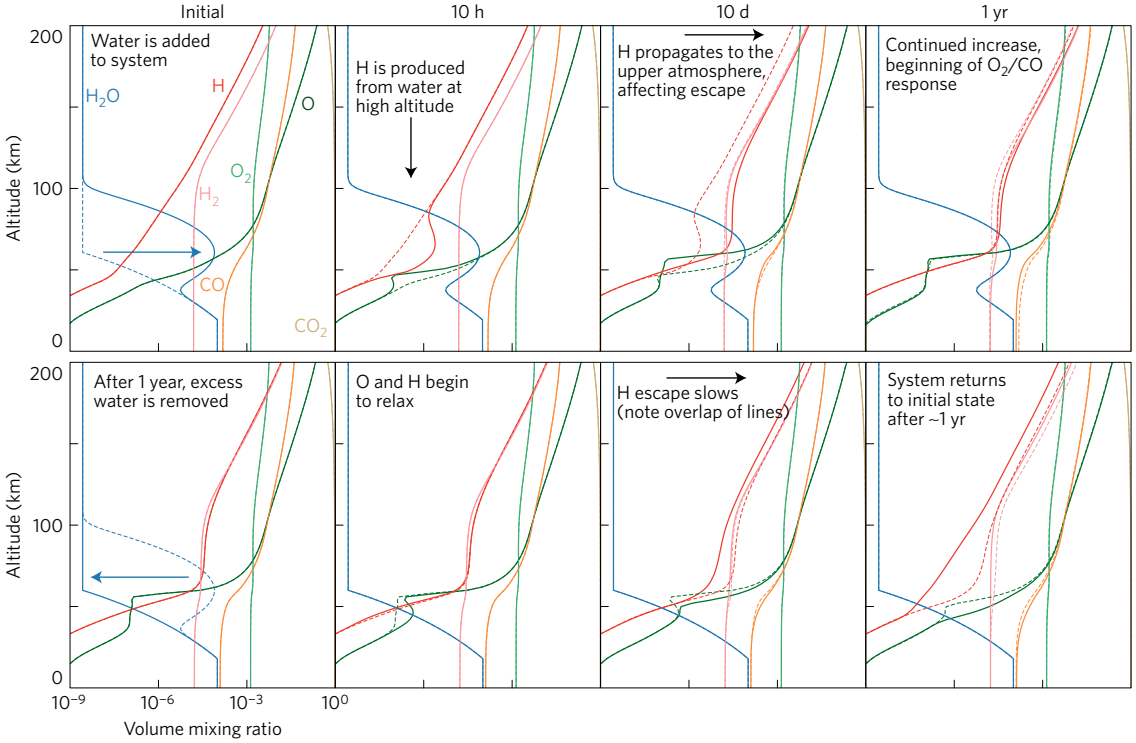

Figure 2 | Time response of the atmosphere to water parcel introduction and subsequent removal. The dashed lines in each panel show the model concentrations from the previous panel. Top row: response of the standard atmosphere to instantaneous introduction of high-altitude water. Bottom row: response of the model to the removal of the water. Both the magnitude and timescale of the H escape response are similar to Mars Express-derived values, as indicated by the increase/decrease of H density at the upper boundary.

in accordance with previous work[14]. These low-altitude changes all represent at least a 10% increase in total atmospheric water content, but the resulting variations in H escape are less than 5% in the first year, minimally affecting H loss. Long-lived perturbations at low altitudes can influence H escape on thousand-year timescales, but do not produce a prompt response (see Supplementary Fig. 3).

By contrast, water introduced in the vicinity of 60–80 km drastically affects H escape on a timescale of weeks, increasing hydrogen loss rates by a factor of several. Subsequent removal of the excess water results in a return to lower escape rates on the same timescale. Transient high-altitude water is thus a plausible source for some portion of the variations in atmospheric escape observed by Mars Express in autumn 2007, which observed at least an order of magnitude exponential decline over six months, with an *e*-folding timescale near sixty days[18]. This decline is likely to be the product of changes due to declining upper atmospheric heating[21] and the shutdown of the upper atmospheric water escape pathway we describe here.

Martian atmospheric chemistry and evolution

Our results demonstrate that H escape is strongly affected by the abundance of water at high altitudes, bypassing the steady molecular hydrogen buffer previously thought to control Martian H escape. The large escape rates induced by this water suggest that its presence may be the dominant factor controlling H loss from Mars. The large (>100%) variations we report in escape rate are produced by percent-level variations in the integrated water column, so that detailed knowledge of the vertical distribution of water vapour is required to reconstruct H escape from Mars over time. Such knowledge may be provided by the ExoMars Trace Gas Orbiter mission[30,31].

Despite the photochemical feedback mechanism that requires the instantaneous escape rate of hydrogen to approach twice that of oxygen on geologic timescales, time-integrated loss of H can exceed that of O, affecting the redox balance of the planet. In our work, H escape is enhanced by a factor of ten within weeks of a perturbation to the water column, but the feedback that returns H escape to twice the O escape rate operates on million-year timescales. This means that even although H and O escape are balanced in equilibrium, short-term dynamics can upset this balance for long periods and result in non-stoichiometric escape. Any short-term increase in upper atmospheric water enhances H escape for millions of years—this potentially includes increases in atmospheric water content resulting from evolution of the obliquity and orbit of the planet[32]. The reverse is also true: removing water from a wet upper atmosphere and never reintroducing it would result in a loss of O relative to H, reducing the atmosphere and planet. The transition from an early warm and wet Mars to the cold and dry planet of today may have resulted in such a change.

The excess H escape revealed by our work may help explain discrepancies between estimates of integrated H loss on Mars and the estimated present-day rates. Estimates of present-day escape rates hover around 4×10^8 cm^{-2} s^{-1}, with seasonal departures to high rates on the order of 10^9 cm^{-2} s^{-1} (refs 9,18–20,33,34). At these rates, between 10 and 100 m of water equivalent would be removed over Martian history, depending on the duty cycle of high-escape-rate periods. The global inventory of water has been estimated at perhaps 34 m (ref. 17), so that if estimates of 80–85% loss from lower atmospheric D/H ratios[4] are correct Mars would have initially had between 180–150 m of water. There is therefore a gap between present-day estimates of H loss and the isotope record of integrated loss, suggesting that excess H escape induced by high-altitude water or a more reducing early atmosphere (for example, ref. 35) would be required to explain the evolution of Mars.

The escape pathway we introduce here can help to reproduce variations in contemporary hydrogen escape from Mars, explaining seasonal variation unaccounted for in standard models. Ongoing efforts to understand the history of Martian volatile loss, including

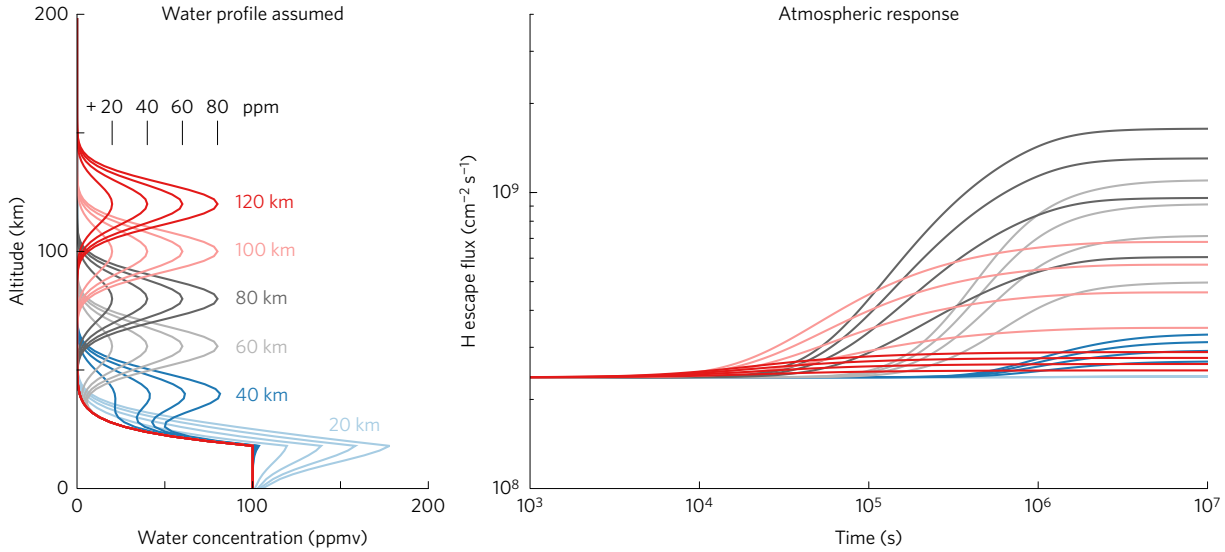

Figure 3 | Sensitivity of atmospheric response to altitude and magnitude of the water parcel injected. Left: water vapour profiles instantaneously introduced into the standard water photochemistry, coloured by altitude of injection. Right: response of atmospheric escape to water introduction. Within each altitude group, magnitude of response is intuitive: more water injection results in a larger impact on escape rates. Timescale of escape response decreases uniformly with altitude, but the magnitude of the response is maximized near 80 km as a balance between increasing ease of water photodissociation and transport to the exobase and decreasing atmospheric density and hence perturbation content. For numerical details and the long-term response of the atmosphere, see the Supplementary Methods.

the Mars Atmosphere and Volatile EvolutioN mission[1], will need to account for this pathway going forward. Future modelling efforts should more completely explore the response of the atmosphere to realistic variability in upper atmospheric water. To aid such modelling, attention must be focused on understanding the source, extent, and longevity of high-altitude water, not only to better constrain Mars atmospheric dynamics, but also to understand the long-term desiccation and oxidation history of the planet. Such understanding will help to constrain the degree to which Mars-like planets throughout the Universe can support and sustain habitable environments over their lifetimes.

Methods

Methods, including statements of data availability and any associated accession codes and references, are available in the online version of this paper.

Received 21 March 2016; accepted 23 December 2016; published online 30 January 2017

References

1. Jakosky, B. M. *et al*. The Mars Atmosphere and Volatile Evolution (MAVEN) mission. *Space Sci. Rev.* 3–48 (2015).
2. Owen, T., Maillard, J. P., de Bergh, C. & Lutz, B. L. Deuterium on Mars—the abundance of HDO and the value of D/H. *Science* **240,** 1767–1770 (1988).
3. Mahaffy, P. R. *et al*. The imprint of atmospheric evolution in the D/H of Hesperian clay minerals on Mars. *Science* **347,** 412–414 (2014).
4. Villanueva, G. L. *et al*. Strong water isotopic anomalies in the Martian atmosphere: probing current and ancient reservoirs. *Science* **348,** 218–221 (2015).
5. Krasnopolsky, V. A. Variations of the HDO/H_2O ratio in the Martian atmosphere and loss of water from Mars. *Icarus* **257,** 377–386 (2015).
6. McElroy, M. B. & Donahue, T. M. Stability of the Martian atmosphere. *Science* **177,** 986–988 (1972).
7. Parkinson, T. D. & Hunten, D. M. Spectroscopy and aeronomy of O_2 on Mars. *J. Atmos. Sci.* **29,** 1380–1390 (1972).
8. Nair, H., Allen, M., Anbar, A. D., Yung, Y. L. & Clancy, R. T. A photochemical model of the Martian atmosphere. *Icarus* **111,** 124–150 (1994).
9. Zahnle, K., Haberle, R. M., Catling, D. C. & Kasting, J. F. Photochemical instability of the ancient Martian atmosphere. *J. Geophys. Res.* **113,** 11004 (2008).
10. Lefèvre, F. *et al*. Heterogeneous chemistry in the atmosphere of Mars. *Nature* **454,** 971–975 (2008).
11. Krasnopolsky, V. A. Solar activity variations of thermospheric temperatures on Mars and a problem of CO in the lower atmosphere. *Icarus* **207,** 638–647 (2010).
12. Krasnopolsky, V. A. & Feldman, P. D. Detection of molecular hydrogen in the atmosphere of Mars. *Science* **294,** 1914–1917 (2001).
13. Krasnopolsky, V. A. Mars' upper atmosphere and ionosphere at low, medium, and high solar activities: implications for evolution of water. *J. Geophys. Res.* **107,** 5128 (2002).
14. Krasnopolsky, V. A. Photochemistry of the Martian atmosphere: seasonal, latitudinal, and diurnal variations. *Icarus* **185,** 153–170 (2006).
15. Liu, S. & Donahue, T. The regulation of hydrogen and oxygen escape from Mars. *Icarus* **28,** 231–246 (1976).
16. Lammer, H. *et al*. Loss of water from Mars. *Icarus* **165,** 9–25 (2003).
17. Carr, M. H. & Head, J. W. Martian surface/near-surface water inventory: sources, sinks, and changes with time. *Geophys. Res. Lett.* **42,** 726–732 (2015).
18. Chaffin, M. S. *et al*. Unexpected variability of Martian hydrogen escape. *Geophys. Res. Lett.* **41,** 314–320 (2014).
19. Clarke, J. T. *et al*. A rapid decrease of the hydrogen corona of Mars. *Geophys. Res. Lett.* **41,** 8013–8020 (2014).
20. Bhattacharyya, D., Clarke, J. T., Bertaux, J.-L., Chaufray, J-Y. & Mayyasi, M. A strong seasonal dependence in the Martian hydrogen exosphere. *Geophys. Res. Lett.* **42,** 8678–8685 (2015).
21. Chaufray, J.-Y. *et al*. Variability of the hydrogen in the Martian upper atmosphere as simulated by a 3D atmosphere-exosphere coupling. *Icarus* **245,** 282–294 (2015).
22. Maltagliati, L. *et al*. Evidence of water vapor in excess of saturation in the atmosphere of Mars. *Science* **333,** 1868–1871 (2011).
23. Maltagliati, L. *et al*. Annual survey of water vapor vertical distribution and water-aerosol coupling in the Martian atmosphere observed by SPICAM/MEx solar occultations. *Icarus* **223,** 942–962 (2013).
24. Fox, J. L. The chemistry of protonated species in the Martian ionosphere. *Icarus* **252,** 366–392 (2015).
25. Spiga, A., Faure, J., Madeleine, J.-B., Maattanen, A. & Forget, F. Rocket dust storms and detached dust layers in the Martian atmosphere. *J. Geophys. Res.* **118,** 746–767 (2013).
26. Rafkin, S. C. The potential importance of non-local, deep transport on the energetics, momentum, chemistry, and aerosol distributions in the atmospheres of Earth, Mars, and Titan. *Planet. Space Sci.* **60,** 147–154 (2012).
27. Navarro, T. *et al*. Global climate modeling of the Martian water cycle with improved microphysics and radiatively active water ice clouds. *J. Geophys. Res.* **119,** 1479–1495 (2014).
28. McElroy, M. B., Kong, T. Y. & Yung, Y. L. Photochemistry and evolution of Mars atmosphere: a Viking perspective. *J. Geophys. Res.* **82,** 4379–4388 (1977).

29. Fox, J. L. & Hać, A. B. Photochemical escape of oxygen from Mars: a comparison of the exobase approximation to a Monte Carlo method. *Icarus* **204,** 527–544 (2009).
30. Vandaele, A. *et al*. Science objectives and performances of NOMAD, a spectrometer suite for the ExoMars TGO mission. *Planet. Space Sci.* **119,** 233–248 (2015).
31. Korablev, O. I. *et al*. ACS experiment for atmospheric studies on ExoMars-2016 orbiter. *Solar Syst. Res.* **49,** 529–537 (2015).
32. Laskar, J. *et al*. Long term evolution and chaotic diffusion of the insolation quantities of Mars. *Icarus* **170,** 343–364 (2004).
33. Anderson, D. E. Jr & Hord, C. W. Mariner 6 and 7 ultraviolet spectrometer experiment: analysis of hydrogen Lyman-alpha data. *J. Geophys. Res.* **76,** 6666–6673 (1971).
34. Chaufray, J. Y., Bertaux, J. L., Leblanc, F. & Quémerais, E. Observation of the hydrogen corona with SPICAM on Mars Express. *Icarus* **195,** 598–613 (2008).
35. Ramirez, R. M. *et al*. Warming early Mars with CO_2 and H_2. *Nat. Geosci.* **7,** 59–63 (2014).

Acknowledgements

The photochemical model was developed with support from NASA NESSF NNX11AP49H, NASA MDAP NNX14AM20G, and a NASA Astrobiology Institute Early Career Collaboration Award.

Author contributions

M.S.C. developed the model and performed the analysis. J.D. oversaw development of and contributed to the model. All authors contributed to interpretation of the results and their presentation.

Additional information

Supplementary information is available in the online version of the paper. Reprints and permissions information is available online at www.nature.com/reprints. Correspondence and requests for materials should be addressed to M.S.C.

Competing financial interests

The authors declare no competing financial interests.

Methods

In the photochemical model, the continuity equation

$$\frac{\partial n}{\partial t} = P - L - \frac{\partial \Phi}{\partial z}$$

is solved for the density n of 16 species across 99 altitude bins simultaneously as a function of the chemical production and loss rates P and L and the vertical number density flux Φ. These fluxes are computed for each species using the diffusion equation

$$\Phi = -(D+K)\frac{\mathrm{d}n}{\mathrm{d}z} - \left[D\left(\frac{1}{H} + \frac{1+\alpha_T}{T}\frac{\mathrm{d}T}{\mathrm{d}z}\right) + K\left(\frac{1}{H_a} + \frac{1}{T}\frac{\mathrm{d}T}{\mathrm{d}z}\right)\right] n$$

where D is the binary diffusion coefficient of the species through CO_2, K is the eddy diffusion coefficient, and $H = kT/mg$ is the species-specific atmospheric scale height, with k being Boltzmann's constant, T the atmospheric temperature, m the species-dependent mass, and g the local acceleration of gravity. H_a is the neutral atmospheric scale height, computed using the mean mass of the atmosphere at each altitude, and α_T is the thermal diffusion coefficient. Molecular and thermal diffusion coefficients were adopted from ref. 36. The eddy diffusion coefficient used is taken from ref. 37 (profile K1), and has a value of 10^6 cm^2 s^{-1} below 60 km altitude, and 2×10^{13} (n[cm^{-3}])$^{-1/2}$ cm^2 s^{-1} above. Each species is tracked on an altitude grid from 0 to 200 km, with a spacing of 2 km.

The magnitude of the assumed eddy diffusion does not strongly affect our results. We ran all modelled cases three times, once with the standard eddy diffusion profile, and once each with the eddy diffusion multiplied or divided by a factor of two. Changing the eddy diffusion by a factor of two in either direction produces roughly a factor of two change in the H escape response. Interestingly, this change goes in the opposite sense than might be expected, with increased eddy diffusion leading to lower H escape enhancements, primarily due to more efficient transport of HO_2 from the location of the introduced water to lower altitudes where it produces H_2 less likely to diffuse to the upper atmosphere and affect escape.

Reaction rates, cross-sections, and quantum yields were drawn from a wide survey of the photochemical literature, based on work performed by ref. 38. Most of these data are compiled by ref. 39, but some small differences arising from more accurate measurements or calculations not reviewed there were incorporated in the present calculations. These new rates and cross-sections do not have a significant impact on the atmospheric chemistry. Similarly, a recent proposal that CO_2 photodissociation can directly produce O_2 (ref. 40) has a negligible effect on the chemistry of the Mars atmosphere, because the quantum yield of this pathway is only 5% and the wavelengths required to access it are shorter than 112 nm.

For some simple molecules such as H_2, photodissociation cross-sections were taken from ref. 41, as ref. 39 does not tabulate cross-sections for these species.

The chemical reaction network and rates used are described in Supplementary Table 1, and the model boundary conditions are described in Supplementary Table 2.

At the top of the atmosphere, only three species have an escaping boundary condition: O, assumed to escape at a seasonally averaged fixed rate as a result of near-constant photochemical escape, with rates matching those in ref. 8; and atomic and molecular hydrogen, with a fixed velocity boundary condition corresponding to the Jeans escape effusion velocity at the exobase for an assumed 240 K temperature (see ref. 36). Our results are insensitive to the temperature assumed, as the changes in H escape flux we report here derive from changes in H density rather than temperature.

Important model inputs are shown in Supplementary Fig. 1 and discussed below. The temperature of the atmosphere is taken from ref. 11, with a surface temperature of 211 K and a -1.4 K km^{-1} adiabatic lapse rate of the troposphere to the altitude of the tropopause (70 km), where the profile is isothermal to 120 km and adopts an analytic expression above this height of the form

$$T_{exo} - (T_{exo} - T_{tropo}) \exp\left(-\frac{z - z_{tropo}}{8T_{exo}}\right)$$

where $T_{exo} = 240$ K is the assumed exobase temperature and T_{tropo} and z_{tropo} refer to the temperature and altitude of the tropopause. The saturation vapour pressure of water is taken from ref. 42. Our results are not very sensitive to the selection of temperature profile.

In the current work, we do not self-consistently model the ionosphere, but adopt fixed ionospheric concentrations from the work of ref. 43, the most important of which for the purpose of H chemistry is CO_2^+, which converts molecular H_2 to atomic H in the ionosphere. The solar ultraviolet flux is taken from the Whole Heliosphere Interval[44], which is accurate for quiet sun conditions, and scaled to the distance of Mars. The solar actinic flux is self-consistently attenuated from the top of the atmosphere to the surface, with diffuse scattering assumed to be negligible.

The photochemical model is implemented in Julia[45], a fast language with metaprogramming features. The chemical differential equations and Jacobian of the coupled reaction and transport network are programmatically generated at runtime from an arbitrary chemical reaction network and transport coefficients. Because of this, the model does not depend on the Kinetic Pre-Processor[46], a package widely used for programmatic generation of chemical reaction network analysis code. The Julia code written for this work is comparable in speed to state-of-the-art photochemical models implemented in FORTRAN, being slower by a factor of only several despite the much higher level of the language in use. The entire photochemical model occupies fewer than 1,000 lines, with most of the space occupied by code specifying the reaction network and loading photochemical cross-sections from file.

Code availability. The photochemical model code is available from the corresponding author's github page, https://github.com/planetarymike/chaffin_natgeo_mars_photochemistry.

Data availability. The photochemical model data sources are available from the corresponding author's github page, https://github.com/planetarymike/chaffin_natgeo_mars_photochemistry. Output files representing the complete model runs used to make this paper's figures are available from the corresponding author on request.

References

36. Hunten, D. M. The escape of light gases from planetary atmospheres. *J. Atmos. Sci.* **30,** 1481–1494 (1973).
37. Krasnopolsky, V. A. Photochemistry of the Martian atmosphere (mean conditions). *Icarus* **101,** 313–332 (1993).
38. Deighan, J. *The Effect of an Ozone Layer on Ancient Mars* PhD thesis, Univ. Virginia (2012); http://libra.virginia.edu/catalog/libra-oa:2577
39. Sander, S. P. *et al*. *Chemical Kinetics and Photochemical Data for Use in Atmospheric Studies* Evaluation Number 17 (2011).
40. Lu, Z., Chang, Y. C., Yin, Q.-Z., Ng, C. Y. & Jackson, W. M. Evidence for direct molecular oxygen production in CO_2 photodissociation. *Science* **346,** 61–64 (2014).
41. Huebner, W. & Mukherjee, J. Photoionization and photodissociation rates in solar and blackbody radiation fields. *Planet. Space Sci.* **106,** 11–45 (2015).
42. Washburn, E. W. The vapor pressure of ice and of water below the freezing point. *Mon. Weath. Rev.* **52,** 488–490 (1924).
43. Matta, M., Withers, P. & Mendillo, M. The composition of Mars' topside ionosphere: effects of hydrogen. *J. Geophys. Res.* **118,** 2681–2693 (2013).
44. Woods, T. N. *et al*. Solar irradiance reference spectra (SIRS) for the 2008 whole heliosphere interval (WHI). *Geophys. Res. Lett.* **36,** L01101 (2009).
45. Bezanson, J., Edelman, A., Karpinski, S. & Shah, V. B. Julia: a fresh approach to numerical computing. *ArXiv e-prints* (2014).
46. Damian, V., Sandu, A., Damian, M., Potra, F. & Carmichael, G. R. The kinetic preprocessor KPP-a software environment for solving chemical kinetics. *Comput. Chem. Eng.* **26,** 1567–1579 (2002).